Lab on a Chip

PAPER

View Article Online
View Journal | View Issue

Cite this: *Lab Chip*, 2020, **20**, 1845

Direct loading of blood for plasma separation and diagnostic assays on a digital microfluidic device†

Christopher Dixon, [a] Julian Lamanna[ab] and Aaron R. Wheeler *[abc]

Received 24th March 2020,
Accepted 21st April 2020

DOI: 10.1039/d0lc00302f

rsc.li/loc

Finger-stick blood sampling is convenient for point of care diagnostics, but whole blood samples are problematic for many assays because of severe matrix effects associated with blood cells and cell debris. We introduce a new digital microfluidic (DMF) diagnostic platform with integrated porous membranes for blood-plasma separation from finger-stick blood volumes, capable of performing complex, multi-step, diagnostic assays. Importantly, the samples can be directly loaded onto the device by a finger "dab" for user-friendly operation. We characterize the platform by comparison to plasma generated *via* the "gold standard" centrifugation technique, and demonstrate a 21-step rubella virus (RV) IgG immunoassay yielding a detection limit of 1.9 IU mL^{-1}, below the diagnostic cut-off. We propose that this work represents a critical next step in DMF based portable diagnostic assays—allowing the analysis of whole blood samples without pre-processing.

Introduction

There is great interest in the development of portable disease-diagnostic assays that can be used at the "point of care" (POC). These systems are particularly attractive for application in remote settings in which centralized laboratory testing facilities are not available.[1–5] Finger-stick (and heel-stick) whole-blood sampling methods are convenient for such systems as they are non-invasive and can be used with infants and young children —cases in which an intravenous draw may not be safe to perform. However, whole-blood, a complex fluid that contains substantial volumes of liquid (plasma) and solids (cells and debris), is problematic for many assays because of the severe matrix effects associated with blood cells and their contents.[6] Plasma is thus preferred for POC assays, but plasma generation from whole blood by the conventional "gold standard" method —centrifugation[7]—requires access to external equipment and materials, thus being inconsistent with the POC testing philosophy.[6,8] Microchannel-based methods have been developed to separate plasma from whole blood, relying on diverse mechanisms including hydrodynamic focusing,[9–11] application of external forces (*e.g.*, acoustic, electrical, *etc.*),[12–15] and microfiltration.[16–18] While these are promising alternatives, such systems can become highly complex, particularly when combined with in-line multi-step diagnostic assays.

Digital microfluidics (DMF) is an alternative to conventional microfluidics that is characterized by the manipulation of individual picolitre to microlitre sized droplets on an open surface, often *via* application of electrostatic forces to a planar array of electrodes. When used in the two-plate format, droplets are sandwiched between two substrates—typically a bottom plate consisting of individual driving electrodes—and a top plate made up of a single continuous counter-electrode. The most important advantage of digital microfluidics is its 'reconfigurability', which allows the implementation of diverse applications[19–23] on devices with generic architecture (with little or no change to device design between them). For this reason digital microfluidics has emerged as a popular mechanism for miniaturizing and automating human health-related diagnostic assays,[24–27] and there is at least one report[28] describing the use of a portable DMF diagnostic system at the point of care. We are aware of a single previous paper[29] describing blood-plasma separation in a digital microfluidic device, which relies on a lectin-based agglutination step to immobilize cells, allowing the collection of plasma in a separate droplet for further analysis. The previous report[29] does not include much detail about the blood-plasma separation (*e.g.*, there is no enumeration of cells remaining in the plasma), and samples in this technique were first metered in a "sample transfer pipette" prior to loading onto the device. This is not ideal for POC applications, which

[a] *Department of Chemistry, University of Toronto, 80. St. George Street, Toronto, Ontario, M5S 3H6, Canada. E-mail: aaron.wheeler@utoronto.ca; Fax: +1 416 946 3865; Tel: +1 416 946 3864*
[b] *Donnelly Centre for Cellular and Biomolecular Research, University of Toronto, 160 College Street, Toronto, Ontario, M5S 3E1, Canada*
[c] *Institute for Biomaterials and Biomedical Engineering, University of Toronto, 164 College Street, Toronto, Ontario, M5S 3G9, Canada*

† Electronic supplementary information (ESI) available: ESI includes a document featuring three figures (Fig. S1–S3) and a note (N1), as well a movie file, M1. See DOI:10.1039/d0lc00302f

must be as simple as possible (with minimal user-intervention) to prevent user bias and error.[30,31]

Here we introduce a new digital microfluidic system that allows for automated, on-chip blood-plasma separation. In developing this method, we considered the microfluidic blood-plasma separation techniques reported previously,[9–18] and chose to use microfiltration,[16–18] which aligned best with our goal to generate low-cost, accessible POC devices. Specifically, we introduce methods to integrate porous, paper-like membranes into the DMF device architecture. When ready for use, an aliquot of blood is loaded onto the membrane, and then is wicked into the DMF device such that the filtered plasma can be collected into droplets. Importantly, this new technique effectively bridges the "world to chip" divide[32–34]—there is absolutely no processing of the sample prior to loading it onto the device—the user can simply "dab" a pin-prick of blood onto the membrane, with all subsequent steps, including plasma generation (*via* microfiltration) and other operations, implemented automatically, without user intervention. Here, we describe the characterization of the new technique for blood-plasma separation as it compares to the gold-standard of centrifugal separation,[7] and also describe an alternate configuration in which particles of different sizes are separated in the membrane. Finally, we demonstrate automated blood-plasma separation in-line with automated diagnostic assays, joining just a handful of previous reports[9,11,15,29] of such methods (integrated in any microfluidic format) in the literature. We propose that this new technique will be broadly applicable to many different diagnostic assays for remote POC diagnostic testing.

Materials and methods

Reagents and materials

Unless otherwise specified, reagents were purchased from Sigma Aldrich (Oakville, ON). Deionized water (DI) water had a resistivity of >18 MΩ cm at 25 °C. Tetronic 90R4 was generously donated by Brenntag Canada (Toronto, ON). Novele IJ-220 inkjet printing media and Metalon JS-B25P silver nanoparticle ink were purchased from NovaCentrix (Austin, TX). Glass slides were purchased from S.I. Howard Glass Co., Inc. (Worcester, MA). ITO-PET substrate was purchased from Memcon North America (Stevensville, MI). Acrylic sheets were purchased from McMaster-Carr (Elmhurst, IL). ARcare 92712 double sided tape (top-plate adhesive, TPA and membrane adhesive, MA) was purchased from Adhesives Research, Inc. (Glen Rock, PA). Scotch Brand double sided tape (DMF spacer adhesive, ~100 μm thick) was purchased from Grand & Toy (Toronto, ON). FluoroPel PFC 1101V was purchased from Cytonix, LLC (Beltsville, MD). Whatman qualitative filter paper: grade 1 (filter membrane, FM, ~180 μm thick), red fluorescent polymer microspheres (0.3 μm dia.), and green fluorescent polymer microspheres (9.9 μm dia.) were purchased from Thermo Fisher Scientific (Rockford, IL). Vivid plasma separation membrane GR (plasma separation membrane, SM, ~330 μm thick) and Supor-5000 unsupported polyethersulfone membrane (transport membrane, TM, ~133 μm thick) were purchased from Pall Biotech (Mississauga, ON). Human whole blood (stabilized with EDTA) was purchased from Cedarlane Labs (Burlington, ON). Immunoassay reagents were adapted from the Architect rubella IgG assay kit from Abbott Laboratories (Abbott Park, IL), including RV IgG calibrators and virus-coated paramagnetic particles. SuperBlock Tris-buffered saline, SuperSignal ELISA Femto chemiluminescent substrate comprising stable hydrogen peroxide (H_2O_2) and luminol enhancer solution were purchased from Thermo Fisher Scientific (Rockford, IL) and each supplemented with 0.1% (v/v) Tetronic 90R4. Custom digital microfluidic wash buffer and extraction buffer comprised Dulbecco's phosphate buffered saline (DPBS) supplemented with 0.1% (v/v) Tetronic 90R4. Conjugate working and sample diluent solutions were prepared as described previously.[28]

DMF device fabrication, assembly, and operation

DMF bottom plates were formed by inkjet printing using an Epson C88+ inkjet printer (Seiko Epson Corporation, Suwa, Japan) to deposit Metalon JS-B25 silver nanoparticle ink onto Novele IJ-220 printing media as described previously.[28] The bottom plate featured 77 roughly square interdigitated driving electrodes (2.8 mm × 2.8 mm), 8 reservoir electrodes (7.6 mm × 6.4 mm), and 8 dispensing electrodes (5.6 mm × 2.0 mm) (Fig. 1A). The driving electrodes were arranged in an array of 26 rows containing one, two, or four electrodes. Gaps between adjacent electrodes were designed (in software) to be 150 μm and the widths of traces connecting electrodes to contact pads were designed to be 100 μm. After printing, bottom plates were diced and affixed to glass slides and coated with dielectric and hydrophobic layers as described previously.[28]

After fabrication, bottom plates were modified to include porous membrane structures. Most devices (used for blood-plasma separation) featured a three-piece membrane assembly as shown in ESI† Fig. S1A. First, a 76 mm × 51 mm strip of transport membrane (TM) was cut from the source, and a ~2 mm-wide line of wax was deposited along the short axis, 10 mm from the edge, using an electric kistka wax pen (Folk Impressions, Franklin, MI). The TM strip was warmed on a hot-plate at 110 °C for 30 seconds to allow the wax to impregnate the material, and then was cooled and diced into 40 mm × ~2 mm sections [leaving a ~2 mm-wide impregnated wax plug (WP) on one end] using a Silhouette CAMEO 3 craft cutter (Silhouette America, Inc., Lindon, UT). Second, 12.6 mm × 12.6 mm sections of plasma separation membrane (SM) were cut using a scalpel and a 3D-printed stencil. Third, membrane adhesive (MA) gaskets were formed using the craft cutter to form 12 mm × 12 mm-wide pieces that resembled a straight-lined "C" with serifs, featuring a width of 2.0 mm, and an opening and depth of 4.0 mm and 8.0 mm, respectively. To assemble the structure, an MA

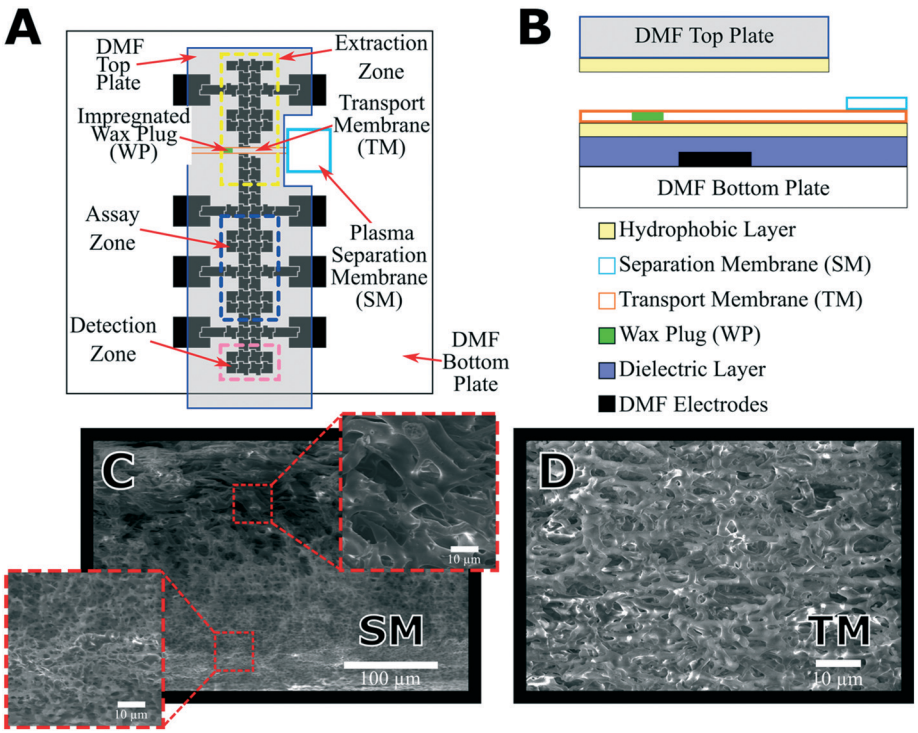

Fig. 1 Digital microfluidic device for blood-plasma separation and diagnostic assays. (A) Top-view schematic of a complete two-plate device with inkjet-printed bottom plate (black outline) and ITO-PET top plate (blue outline), plasma separation membrane (SM, turquoise outline) for trapping red blood cells, transport membrane (TM, orange outline) for delivery of filtered plasma into electrode array, and impregnated wax plug (WP, green) to limit the flow of plasma in the TM. Plasma separation is performed in the extraction zone (yellow dashed box), in-line ELISAs in the assay zone (blue dashed box), and chemiluminescent readout in the detection zone (pink dashed box). (B) Cross-section image (not to scale) of a complete two-plate device bearing a DMF driving electrode (black) coated with dielectric (purple) and hydrophobic (yellow) layers. (C) A cross-section scanning electron microscopy (SEM) micrograph of a SM showing asymmetric structure. Magnified insets (red dashed outline) show larger pores at the top (right) and smaller pores (left) at the bottom of the SM. (D) A cross-section SEM micrograph of a TM.

gasket was placed on the DMF bottom plate centered between two reservoir electrodes, with the opening of the "C" facing the driving-electrode array. A TM was then positioned on the DMF bottom plate such that the non-waxed end penetrated the MA gasket, oriented such that the long-axis of the membrane crosses a driving-electrode row with one electrode. A SM was then placed on top of the TM in alignment with the MA gasket, and the edges of the SM (1 mm) were crimped with a custom 3D-printed tool. Other devices (used for size-based particle separation) featured a single-piece membrane assembly as shown in ESI† Fig. S1B. In these devices, 40 mm × ~2 mm filter membrane (FM) strips were prepared (and positioned on DMF bottom plates) identically to the TM (above), except with WPs on both ends. In some cases, membranes (SM or TM) were evaluated by scanning electron microscopy (SEM), with images acquired *via* a Quanta FEG 250 SEM (FEI, Hillsboro, OR) in secondary electron mode with an accelerating voltage of 10 kV. In these experiments, the samples were frozen in liquid nitrogen (to preserve porous structure) and cut with a razor blade to reveal the cross-section prior to analysis.

DMF top plates were formed from ITO-PET substrates coated with FluoroPel PFC 1101V as described previously.[25] After coating, ITO-PET substrates were covered with a protective covering of Parafilm M (Bemis Company, Inc.), adhered to a ~48 μm thick top-plate adhesive (TPA) layer, and then diced into their final shapes (75 mm × 32 mm with a 14.7 mm × 5.7 mm indent on one side) with the craft cutter. Top plate backing—formed from 1.5 mm thick acrylic—was cut into the same (or similar) shape as the ITO-PET substrate with a Hobby Series 20 × 12 CO_2 laser cutter (Full Spectrum Laser, Las Vegas, NV), which was pressed on to the TPA layer to complete the top plate. Fully assembled DMF devices (Fig. 1) were formed by removing the Parafilm from a top plate and joining it to a bottom plate *via* one or two layers of DMF spacer adhesive—aligning the cut-out in the top plate with the SM on the bottom plate. This resulted in an inter-plate gap of around 100 μm or 200 μm and a unit droplet (*i.e.*, a droplet covering a single driving electrode) volume of ~0.65 μL or ~1.3 μL.

Devices were interfaced through pogo-pin connectors to a "Measles Rubella-Box" (MR Box) digital microfluidic control system, which is described in detail elsewhere.[28] Droplets were actuated by applying a force of ~25 μN mm^{-1} (sine waves ~100 V_{RMS} at 10 kHz) in a pre-programmed sequence using the open-source MicroDrop 2.0 software.[35] The applied force was determined to be below the velocity-saturation force for the liquids used here using the methods described

by Swyer *et al.*[36] In some experiments, droplet positions were monitored by imaging with a cell phone camera mounted to a SZ61 stereo microscope (Olympus Corp., Tokyo, Japan) using a custom 3D-printed mount. At various times, devices were removed from the MR Box and evaluated *via* an OptixCam D3K2-14 digital camera (Microscope LLC, Roanoke, VA) mounted on an IX71 inverted microscope (Olympus Corp., Tokyo, Japan) with visible or UV illumination (the latter from a X-Cite 120 fluorescence illuminator, Excelitas Technologies Corp., Waltham, MA), or with a cell phone camera under visible or UV illumination (the latter from a Globe Electric 28020 fluorescent lamp, Globe Electric, Pointe-Claire, QC).

Blood-plasma separation

For DMF blood-plasma separation, an assembled device bearing a TM and SM (ESI† Fig. S1A) was interfaced with the MR Box and reagents were loaded into the reservoirs, in preparation for a four-step procedure. (1) A fully assembled plasma separation device is interfaced with the MR Box. (2) Droplets of extraction buffer were dispensed onto the array in the extraction zone and merged to form a five-unit extraction droplet (with volume ~6.5 μL or ~3.25 μL for devices formed with the different inter-plate spacers), after which a sample (often 55 μL but occasionally other volumes) of whole blood was pipetted or "dabbed" from a gloved finger onto the SM. (3) After about 3 minutes the extraction droplet was driven through the TM perpendicular to the long axis of the membrane. (4) After passing through the membrane, the droplet was either actuated to the assay zone for analysis on-chip or was recovered with a pipette for analysis off-chip. Plasma was separated from whole blood off-chip by centrifuge, dispensing 0.5 mL into a 1.5 mL microcentrifuge tube and spinning it down at 2000 × *g* for 15 minutes in an AccuSpin™ Micro 17 centrifuge (Thermo Fisher Scientific, Rockford, IL). Separated plasma was recovered using a pipette and stored for analysis.

Characterization of loading and extraction/dilution

Loading experiments were conducted in devices with inter-plate gaps of 200 μm, following the 4-step blood-plasma separation procedure indicated above, except with variations in blood volume loaded onto the SM. Absorbances were measured at 280 nm (relative to the absorbance of neat solvent) using a NanoDrop 1000 spectrophotometer (Thermo Fisher Scientific, Waltham, MA) and were converted to protein concentrations (according to the NanoDrop Protein A280 product insert) for 3 μL aliquots of extract collected after running the procedure. Extraction/dilution experiments were conducted in devices with inter-plate gaps of 100 μm, following the 4-step blood-plasma separation procedure indicated above, except with tracer solution [0.1% (v/v) blue dye (McCormick Canada, London, ON) in DI water] substituted for blood. Absorbances were measured at 630 nm (relative to the absorbance of neat solvent) using a NanoDrop 1000 for 3 μL aliquots of tracer solution and extract solution before and after running the procedure.

Characterization of blood-plasma separation

Plasma samples from replicates of whole blood (generated *via* centrifugation or DMF in devices with inter-plate gaps of 200 μm) were examined for (i) hematocyte numbers, (ii) hemoglobin content, and (iii) native protein recovery, as described below. Examination (i) was carried out by inspecting 5 μL samples (diluted 1 : 1) using a Bright-Line hemocytometer (Hausser Scientific, Horsham, PA) under a DM 2000 upright microscope (Leica Microsystems, Wetzlar, Germany). Examination (ii) was carried out by measuring absorbance of 3 μL samples at 414 nm using a NanoDrop 1000 (relative to the absorbance of neat solvent). Examination (iii) was carried out by processing and analyzing 3 μL samples with a bromocresol green (BCG) albumin assay kit (Thermo Fisher Scientific, Waltham, MA) per manufacturer's instructions, using a 96-well plate in a PHERAstar microplate reader (BMG Labtech, Ortenburg, Germany). The final values for data in examinations (i–iii) determined from plasma samples generated by DMF were adjusted for dilution by multiplying by factor k (eqn (1)),

$$k = \frac{V_d}{V_m} = \frac{n_u \cdot h_g \cdot A_u}{\phi \cdot L_p \cdot W_p \cdot H_p} \quad (1)$$

where V_d is the volume of the extraction droplet, V_m is the volume of plasma eluted from the membrane, n_u is the number of unit droplets that are merged to form the extraction droplet, h_g the inter-plate gap, A_u the area covered by a single unit-droplet, ϕ the membrane porosity, and L_p, W_p, and H_p, are the length, width, and height of the extracted portion of the TM. For examinations (i–iii), n_u = 5, A_u = 6.69 mm^2, h_g = 200 μm, ϕ = 0.70, L_p = 4.94 mm, W_p = 2.00 mm, H_p = 0.133 mm, V_d = 6.7 μL and V_m = 0.92 μL.

On-chip particle separation

For particle-separation experiments, an assembled device bearing a FM (ESI† Fig. S1B) and an inter-plate gap of 200 μm was interfaced with the MR Box and reagents [including a suspension of red (0.3 μm dia.) and green (9.9 μm dia.) fluorescent particles (formed from a 1 : 1 mixture of stock suspensions)] were loaded into reservoirs, in preparation for a five-step procedure. (1) Two double-unit droplets of extraction buffer were dispensed onto the array and wicked into the FM, with excess liquid directed to waste [note that the nominal "dry" FM thickness is 180 μm (slightly smaller than the inter-plate gap), but upon saturating in this step, it swells such that the inter-plate gap is completely blocked]. (2) Two double-unit droplets and one single-unit droplet of particle suspension were dispensed onto the array and merged to form a sample droplet. (3) The sample droplet was driven through the FM perpendicular to the long axis of the membrane. (4) Two double-unit droplets and one single-unit droplet of extraction buffer were dispensed onto the array

and merged to form an extraction droplet. (6) The extraction droplet was driven through the FM in the opposite direction of the sample droplet.

RV IgG ELISA

RV IgG DMF ELISAs with on-chip blood-plasma separation were implemented in 21 steps in devices with inter-plate gaps of 200 μm. (1–4) Plasma was generated on-chip in the extraction zone from whole blood (containing RV IgG calibrator spiked at concentrations of 0, 7.5, 15, and 30 IU mL^{-1}) following the protocol described above. (5) A double-unit droplet of virus-coated paramagnetic particles (1.5×10^8 mL^{-1}) was dispensed from a reservoir to the assay zone, the particles immobilized using the built-in servo motor-controlled, rotating magnetic lens in the MR Box,[28] and the supernatant droplets was moved to waste. (6) A double-unit droplet of separated plasma from the extraction zone was actuated to the assay zone, delivered to the paramagnetic particles, actively mixed for 7 minutes, after which the particles were immobilized and the supernatant moved to waste. (7) A double-unit droplet of wash buffer was dispensed and delivered to the paramagnetic particles, actively mixed for 30 seconds, after which the particles were immobilized and the supernatant moved to waste. (8–12) Step 7 was repeated five times. (13) A double-unit droplet of conjugate solution (containing HRP-conjugated anti-human IgG) was dispensed, delivered to the particles, and actively mixed for 5 minutes. (14–17) Step 7 was repeated four times. (18) A double-unit droplet of wash buffer was dispensed and delivered to the paramagnetic particles, and actively mixed for 10 seconds. The droplet was actuated to the detection zone, immobilized, and the supernatant moved to waste. (19) A single-unit droplet of luminol enhancer solution was dispensed and delivered to the paramagnetic particles, and actively mixed for 10 seconds. (20) A single-unit droplet of stable H_2O_2 solution was dispensed and delivered to the droplet containing the paramagnetic particles, and actively mixed for 80 seconds. (21) The resulting chemiluminescence was measured (120 s collected at 60 Hz, recording the mean for the final 40 seconds) using the integrated H10721-01 photomultiplier tube (Hamamatsu Photonics K.K., Hamamatsu, Japan) in the MR Box.[28] In each experiment, steps 5–20 were performed in parallel on two separate sample droplets in the assay zone (such that two samples were processed at the same time), after which they were analyzed (step 21) sequentially. Each assay with on-chip blood-plasma separation was repeated at least three times for each concentration of IgG spiked into whole blood (0, 7.5, 15, 30 IU mL^{-1}). The data were plotted as a function of concentration and fit to a linear regression model. The limits of detection (LOD) and quantification (LOQ) were calculated as the concentrations (according to the fitted function) corresponding to the mean signal generated from blank measurements plus 3 (LOD) or 10 (LOQ) times the standard deviation of the blank measurements.

RV IgG DMF ELISAs without blood-plasma separation (prepared "off-chip") were implemented using a variation of the 21-step procedure described above. In these experiments, whole blood samples were manually diluted 1 : 10 in sample diluent and spiked such that (after dilution) they contained 15 IU mL^{-1} IgG. To initiate the experiments, a 7.5 μL aliquot was pipetted into a designated reservoir on a device without membranes. These assays effectively began with step (5), and the sample in step (6) was a double-unit droplet of diluted blood that was dispensed onto the array. The sample volumes evaluated in these experiments (V_{du} = 2.6 μL) were larger than the sample volumes eluted from the membrane in blood-plasma separation experiments (V_m = 0.91 μL); thus, for comparison, the off-chip blood dilution measurements were scaled by a factor of V_m/V_{du} = 0.35.

Results and discussion

Digital microfluidic blood-plasma separation

Plasma generation from finger-stick volumes of blood is a long-standing challenge for microfluidic POC devices.[37] We chose to explore integrating porous membranes with digital microfluidics for this purpose, which we hypothesized would allow for seamless separation of cells and other solids from blood to generate plasma, as well as providing a convenient mechanism to bridge the "world-to-chip" gap between sample and device. We are aware of one previous report[38] of a "membrane" in a DMF device comprising arrays of photolithographically defined pillars, and a second report[39] of a membrane used as a capillary-pump (positioned away from the path of droplet movement). As far as we are aware, the DMF devices described here are the first to incorporate a paper-like membrane (*i.e.*, a pre-formed, dense, solid material featuring an asymmetric/tortuous fluid-flow path) into the path of droplet movement.

The new device design is shown in Fig. 1A and B. In preliminary work, it was discovered that there are at least three key components that are required for device operability: a plasma separation membrane (SM), a transport membrane (TM), and a fluid-flow barrier. The first component, the SM, is formed from a commercial product that features an asymmetric structure in which pores are large on one side and become smaller as fluid passes through to the other side (Fig. 1C). Including this type of material, which allows hematocytes to be gently trapped in the larger pores (avoiding shear-induced lysis) while filtered plasma flows freely into the smaller voids below, was found to be critical for plasma separation performance. After some trial-and-error, the design shown in Fig. 1 was adopted, with the SM located just outside the top plate, which allows for direct sample introduction by pipette or by "dab" (see below). The second component, the TM, is simply a carrier material, designed to wick plasma onto the array of electrodes. A number of materials were evaluated for this purpose including blocked cellulose, blocked nitrocellulose, and glass fibre; we ultimately chose a hydrophilic polyethersulfone

membrane,[40] as it features low bio-molecule binding (<1%) and an average pore size of 5.0 μm (Fig. 1D), which (as described previously for other applications[41]) was found to support rapid, reproducible fluid flow. Finally, the third critical component, a fluid-flow barrier, was found to be important to stop the flow of sample and other reagents through the membrane. In the devices described here, this role was filled by an impregnated wax plug (WP). The SM, TM, and WP were straightforward to form (using a commercial craft-cutter and wax pen) and assemble, as shown in ESI† Fig. S1A.

Fig. 2 depicts the four-step process for generating plasma in the new system. Briefly, first, a fully assembled plasma separation device is interfaced with the MR Box (Fig. 2i). Second, a droplet of extraction buffer is dispensed onto the array, and a sample of blood is loaded into the SM (Fig. 2ii). As illustrated, cells are collected on the SM, and the plasma flows through the TM until it reaches the WP, a process that takes approximately 3 minutes. [When sample wicks through the TM, it undergoes a colour change, which was used here to (qualitatively) signal to the operator that loading was complete. In the future, it may be possible to use the capacitance measurements that are integral to the DMF control system used here[35] to determine precisely when the sample has been fully loaded.] Third, the extraction buffer droplet is driven through the TM (Fig. 2iii), a process that takes approximately 30 seconds, and fourth, the plasma-containing droplet separates from the membrane (Fig. 2iv), where it is ready for further processing and analysis. In sum, the total time to plasma generation is approximately 4 minutes—a duration that is on par with other microfluidic membrane filtration separation methods.[16–18]

In developing the new method described here, four observations stood out to us as being particularly interesting or important. The first observation is the 'ease' of sample introduction into the device. As shown in ESI† Fig. S2A and ESI† Movie M1, samples can be "dabbed" onto the SM directly from a finger, effectively bridging the "world-to-chip divide" that has plagued the microfluidic community over the years.[32–34] Likewise, the system was designed to be "sample volume agnostic"—that is, as long as the minimum sample volume needed to saturate the TM is applied, the technique "self-meters" a constant amount of plasma onto the device for analysis. [In the present design the minimum volume is ~50 μL, chosen to match the sample size generated by common finger-prick protocols,[42] but in the future this could be made larger or smaller by changing the dimensions or the porosity of the SM and/or the TM.] For example, as shown in Fig. S2B,† when replicate samples of 50, 55, or 60 μL aliquots of blood are loaded onto the device,

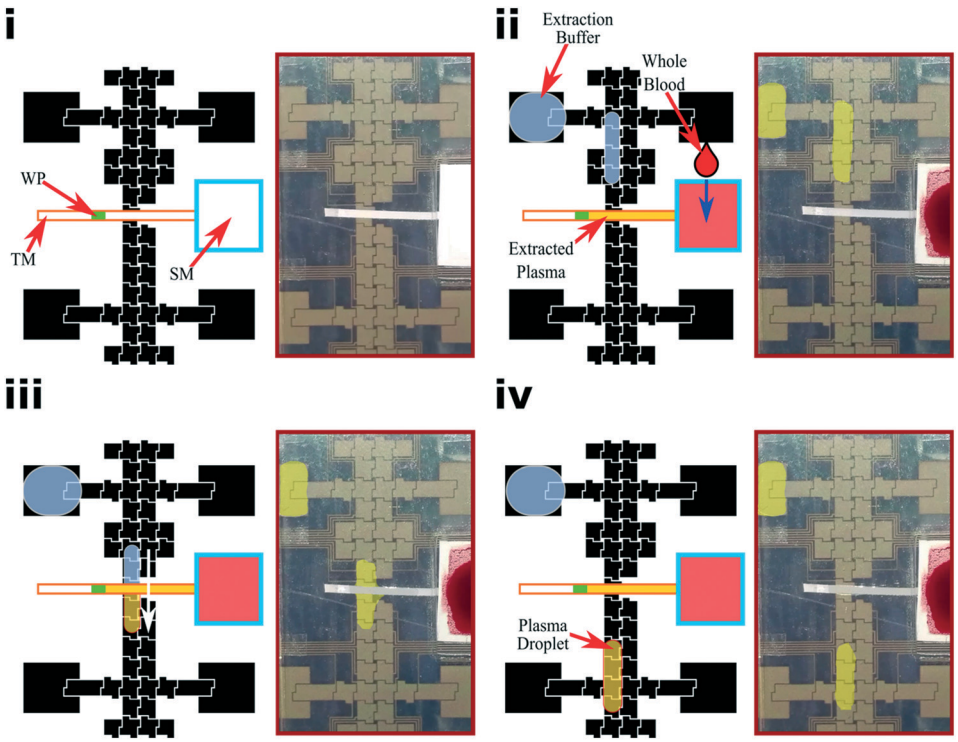

Fig. 2 On-chip DMF blood-plasma separation. Cartoons (left) and photographs (right) illustrating plasma separation on DMF. The droplets in the photographs have been altered with false colouring to make them stand out. (i) A fully assembled plasma separation device is interfaced with the MR Box. (ii) Whole blood is deposited on the SM where blood cells are trapped, and filtered plasma flows through the TM and onto the electrode array, after which extraction buffer is loaded into a reservoir and dispensed onto the electrode array. (iii) Once the TM is saturated with plasma, a droplet of extraction buffer is driven through the TM perpendicular to the length of the membrane. (iv) After separation from the membrane, the plasma-containing droplet is ready for analysis.

the amount of total protein recovered in extract droplets remains the same (one-way ANOVA, $p = 0.84$). Note that the only previous report[28] of a digital microfluidic assay system used in the field (i) collected whole blood samples from patients (of unknown volume) into a tube, followed by (ii) manual dilution and metering into the device by pipette. Likewise, the only previous report[29] of a DMF blood-plasma separation method requires that blood be transferred to the device *via* a "sample transfer pipette". We propose that the new technique, which requires only that the user "dab" a sample (of un-metered volume) of blood onto a device, represents a significant improvement in user-friendliness and accessibility for field work.

The second interesting observation of the new method is the nature of droplet movement 'through' the membrane. The driving forces in DMF are finite and (for successful operation) must overcome a host of resistive forces,[36] including (in this case) the potential tendency of an aqueous droplet to stick to a large, three-dimensional (3D) hydrophilic barrier. There are previous reports of aqueous droplets being driven 'through' 3D hydrophilic barriers (including hydrogels,[43–45] porous polymer monoliths,[46–48] and dried-blood paper punches[49,50]) but in these previous reports, the droplets have been much larger than the barriers, such that the barriers are 'engulfed' by the droplets as they move 'through.' In contrast, this is the first example that we are aware of in which a droplet that is much smaller than a 3D hydrophilic structure is driven 'through' the structure (noting that the aforementioned system featuring an array of pillars[38] is relatively "open" compared to the solid/dense materials described here). In hundreds of experiments, droplets were found to reproducibly move through the barrier (at approximately constant velocity), as illustrated in Fig. 3A. The droplet velocity is reduced about 10-fold during this step relative to other movements on the device (*i.e.*, ~0.4 mm s^{-1} when moving through the barrier, and ~4 mm s^{-1} when not). We speculate that this effect can be attributed to increased resistive forces acting against droplet movement imposed by interactions with the membrane; this is an interesting phenomenon that warrants further study as its mechanics are not completely understood at this time.

The third interesting observation of the new method is the mechanism and quantitation of extraction and dilution of analyte from the TM during extraction. As illustrated by the images in Fig. 3A, the flow of the droplet 'through' the TM appears to be laminar, such that only analytes in the immediate path of the droplet are collected [this is supported by a calculation of Reynold's number < 1 for this system, as per ESI† Note N1]. Furthermore, the volume of the extraction droplet V_d, which can be estimated from electrode and inter-plate gap dimensions, remains approximately the same, before and after extraction. Likewise, the boundaries imposed by the extraction droplet, as well as the dimensions and porosity of the TM allow an estimation of the volume of plasma that is eluted from the membrane V_m. Together, this information allows estimation of the predicted dilution factor, V_m/V_d, which ranged from around 14% to 28% in the devices used here. This estimate is supported by experiments —for example, as shown in Fig. 3B, in replicate experiments with a tracer-dye, the average absorbance (±std. dev. for $n = 3$) of pre-extracted and post-extracted sample was 0.94 ± 0.02 and 0.23 ± 0.04, respectively, suggesting a dilution factor similar to the predicted value for this device of $V_m/V_d \approx 0.28$. Thus, for the experiments described in comparisons with centrifuge-generated plasma (described below), values obtained from the DMF device were adjusted for dilution by multiplying by $k = V_d/V_m$ [eqn (1)]. In the future, different TM and device dimensions might be used to tune the dilution ratio depending on the need.

Finally, the fourth interesting observation of the new method is the fact that the principles of the DMF-membrane device introduced here can be repurposed for use with

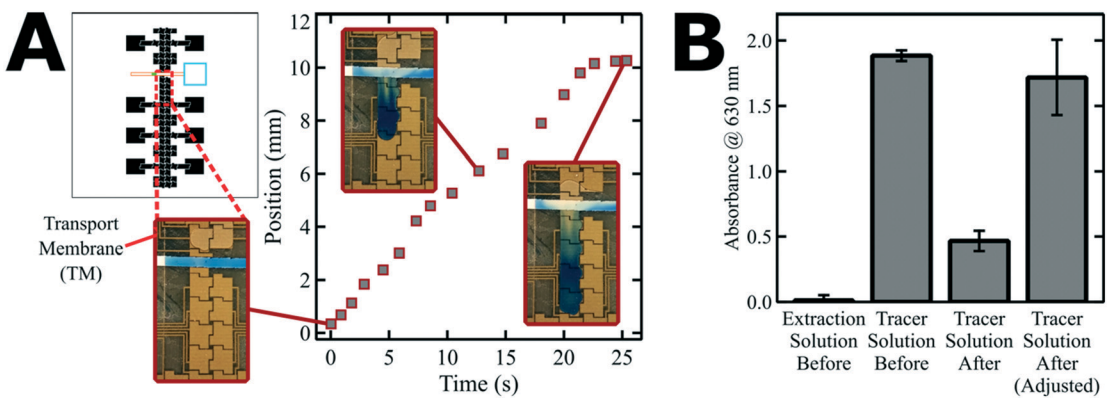

Fig. 3 Characterization of droplet movement through the membrane and extraction/dilution on a DMF blood-plasma separation device. (A) Cartoon of device (left) and representative plot of position as a function of time (right) for an extract droplet being driven through the membrane on a DMF device that had been loaded with tracer solution (aqueous blue dye). The insets (red outlines) show photographs illustrating the states at 0, 13, and 25 s after initiating extraction. (B) Plot of absorbance at 630 nm of extraction solution before initiating extraction (left), tracer solution before extraction (mid-left), extraction droplet (containing tracer) after extraction (mid-right), and extraction droplet after extraction upon adjustment by factor k [eqn (1)] (right). Error bars represent ±1 standard deviation from $n = 3$ replicates.

applications other than blood-plasma separation. For example, we hypothesized that if a filter membrane (FM) bearing a desired pore size were used in place of a transfer membrane, the technique might be capable of separating different sizes of particles into discrete droplets on the array [note: in this case, the SM is not needed, allowing for simpler structure (ESI† Fig. S1B) and operation]. In essence, this application is similar to what was described previously,[38] but on a system that replaces photolithographically defined pillars with an inexpensive, paper-like membrane. In proof-of-concept experiments we chose FM membrane material with pores designed to retain particles that are around 10 μm (or larger) in diameter. As shown in ESI† Fig. S3, when droplets containing a mixture of green 9.9 μm diameter particles and red 0.3 μm diameter particles are passed through the FM, the two particle sizes can indeed be separated into separate aliquots [note that the FM must be pre-saturated with liquid prior to separation]. We speculate it should be possible to separate particles of many different sizes and types by simply selecting FMs with appropriate pore diameters; however, this is beyond the scope of this project, which was focused on the development of blood-plasma separation, with validation experiments described below.

Digital microfluidic blood-plasma separation for clinical applications

After developing a digital microfluidic technique for blood-plasma separation, we evaluated its performance using three commonly cited metrics for plasma separation: cell depletion, hemoglobin content, and protein recovery. In these experiments, we compared the performance of the new technique to that of centrifugation,[7] the "gold standard" technique that is also the most widely used method for blood diagnostics requiring plasma.[51]

The first metric for blood-plasma separation, cell depletion, is the most important; after all, the primary goal of blood-plasma separation is to generate a solution that is largely free from cells. For the tests described here, replicate samples were evaluated and the numbers of red blood cells (RBCs) and other hematocytes present before and after separation were counted using a hemocytometer. Fig. 4A shows the hematocyte count in 1 μL volumes of whole blood before separation, plasma generated *via* centrifugation, and plasma generated *via* DMF on-chip separation. As shown, no cells were observed in the DMF generated plasma across all samples evaluated. This performance compares well with centrifugation, which removed 99.9991% of the cells, and with previously reported microfluidic techniques that depleted 89% to 99.9% of cells.[9–11,14,17] This metric was not reported in the one previous report[29] of a DMF blood-plasma separation.

The second common metric used to evaluate blood-plasma separation is hemoglobin content. Hemoglobin is not present in pure plasma; when detected, it is indicative of hemolysis of RBCs. Hemoglobin is problematic for many applications for a number of reasons, including its peroxidase activity,[52] which can interfere with ELISAs such as the one reported here. In many types of plasma separation, hemolysis is (undesirably) initiated by mechanical stresses such as turbulent shear from high flow rates or close packing of RBCs caused by inefficient filtration.[53] This was the motivation for our use of the asymmetric SM in developing the DMF method, as described above. It is widely accepted that absorbance values at 414 nm (the abs.-max of hemoglobin) of 0.3 units[54,55] (or less) at this wavelength are indicative of plasma that is non-hemolyzed. As shown in Fig. 4B, the DMF-derived plasma has an absorbance of less than 0.3 units—this performance is similar to what has been reported previously for microfluidic blood-plasma separation.[18,29]

The third common metric that is used to evaluate blood-plasma separation is the recovery of protein from blood, often monitored by quantifying the most abundant protein, serum albumin. Filter-based methods are often inferior to centrifugation in this capacity, as proteins can irreversibly

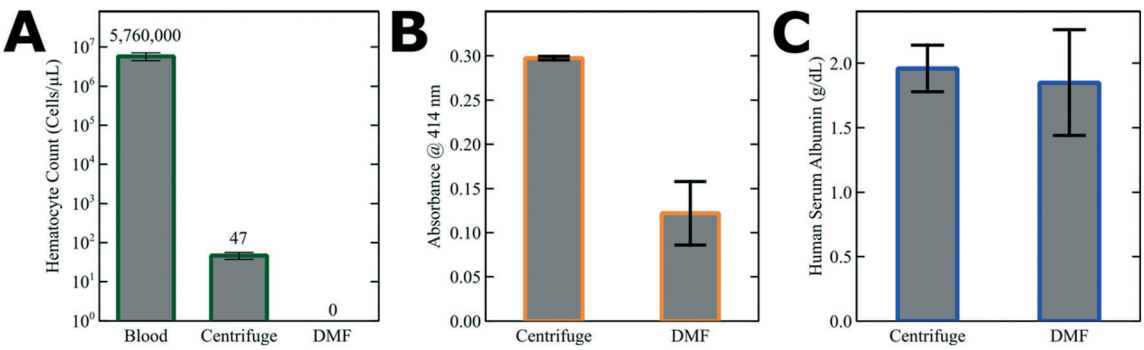

Fig. 4 Comparison of plasma generated *via* on-chip DMF blood-plasma separation *versus* plasma generated from whole blood *via* the "gold standard" centrifugation method. (A) Plot of the density of hematocytes in whole blood (left), and the densities of hematocytes in plasma generated *via* centrifugation (middle) and plasma generated on-chip (adjusted for dilution, right). (B) Plot of absorbance at 414 nm in plasma generated *via* centrifugation (left) and on-chip (adjusted for dilution, right). (C) Plot of human serum albumin concentration in plasma generated *via* centrifugation (left) and on-chip (adjusted for dilution, right). Error bars represent ±1 standard deviation from n = 3, 3, and 5 replicates per condition for plots A, B, and C, respectively.

adsorb to filter materials, reducing the recovery into plasma.[56] This motivated our efforts to select filter materials for the new DMF technique with low non-specific protein binding, as described above. Fig. 4C shows albumin recovery in centrifuge- and DMF-generated plasma is similar, indicating that there is little depletion of protein using the DMF-based method. This performance is comparable to other microfluidic membrane filtration methods that have reported recoveries of 63–110% compared to centrifuged plasma.[16–18] Overall, on the basis of the three metrics represented in Fig. 4 (cell depletion, hemoglobin content, and protein recovery), we are confident that the DMF method produces plasma that is close to being equivalent to the gold-standard technique.

With the ability to generate high-quality cell-free plasma on a DMF device, we turned to evaluating the potential for coupling blood-plasma separation with a multistep diagnostic assay. The rubella virus (RV) is an infectious disease characterized by a mild fever and rash, as well as upper airway inflammation.[57,58] However, the most serious RV complications are caused by its replication in fetal tissues leading to a host of prenatal disorders known collectively as congenital rubella syndrome (CRS).[58] In cases that are at-risk for CRS, it is critical to know the immune status of pregnant mothers, which is determined by quantifying the mother's RV IgG. DMF-based RV IgG assays have been previously demonstrated in the lab[24,25] and in the field at the POC;[28] however, these prior implementations have a critical weakness—a world-to-chip divide in which blood samples must be diluted and metered off-chip prior to loading them into the system for analysis. Thus, the RV IgG assay was a natural choice for us to evaluate the capability of the new, fully integrated system described here.

As illustrated in Fig. 5A, a custom 21-step processing and analysis method was developed to automate blood-plasma separation in-line with quantification of RV IgG. Fig. 5B is a calibration curve generated for blood samples containing 0–30 IU mL^{-1} RV IgG processed in this manner. The data were fit by linear regression, yielding an LOD and LOQ of 1.9 IU mL^{-1} and 3.6 IU mL^{-1}, respectively; importantly, both values are below the diagnostic cut-off of 10 IU mL^{-1} for RV immunity as defined by the World Health Organization,[59] and are similar to what has been reported previously for DMF RV IgG diagnostic assays.[24,25] Finally, blood samples spiked with 15 IU mL^{-1} RV IgG were processed off-chip (diluted 1 : 10 and metered with a pipette) as reported

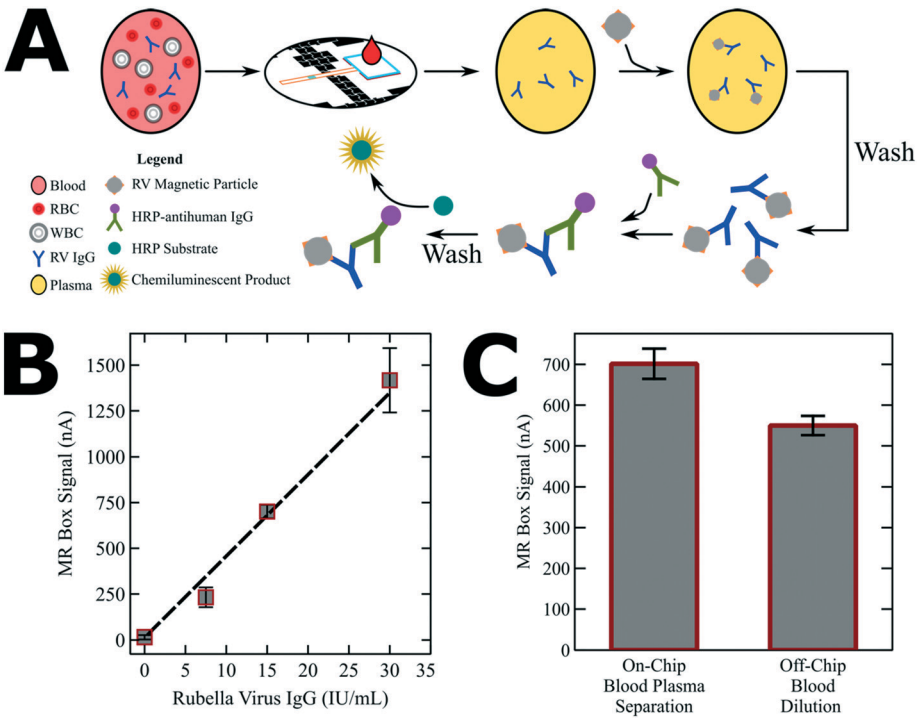

Fig. 5 DMF blood-plasma separation with integrated ELISA for RV IgG. (A) Cartoon outlining key steps in the 21-step scheme. A whole blood sample (light red) is loaded onto the SM on the DMF chip. RBCs (dark red) and WBCs (white) are trapped in the SM while filtered plasma (yellow) containing RV IgG (blue) is extracted into a droplet on the DMF device. Magnetic particles (gray) coated with virus (orange) are mixed with the extracted plasma droplet. Wash buffer droplets remove unbound RV IgG, and IgG-laded particles are mixed with HRP conjugated to antihuman IgG (purple-green). Unbound conjugate is removed with additional wash buffer droplets, followed by introduction of HRP substrate (teal) and then measurement of the resulting chemiluminescence. (B) Plot of chemiluminescence signal (markers) from RV-IgG-spiked blood samples processed as in (A) as a function of concentration. Data were fit with a linear regression (dashed line). (C) Plot comparing the signal generated from blood containing 15 IU mL^{-1} RV IgG with on-chip DMF plasma separation (left) and with off-chip 1 : 10 whole blood dilution containing 15 IU mL^{-1} RV IgG (right, adjusted for sample size). Error bars in (B and C) represent ±1 standard deviation from n = 3 replicates per condition.

previously.[28] As shown in Fig. 5C, the values generated by the two methods were comparable, suggesting that the new technique does not cause substantial perturbations to the existing, field-validated technique.[28]

Conclusion

We introduced a new DMF-based method for integrated blood-plasma separation. As far as we are aware, this is the first digital microfluidic technique that allows for direct sample loading, with no user intervention prior to analysis. Plasma generated using the new method has similar properties relative to that generated *via* the gold standard centrifugation method in terms of cell-depletion, hemolysis, and protein recovery. As a proof-of-concept application, the new integrated platform was used to perform a diagnostic assay on an unprocessed whole blood sample—first generating plasma, then performing a diagnostic ELISA in-line. We propose that the method described here is a general one that should be widely applicable to the growing community of researchers exploring the use of DMF for diagnostic applications.

Author contributions

C. D., J. L, and A. R. W. conceived of the DMF-membrane interface. C. D. developed the method to manufacture the devices and fabricated them with assistance from J. L. C. D. performed the experiments and analyzed the data. C. D. and A. R. W. wrote the manuscript, with input from J. L.

Competing interests

C. D., J. L., and A. R. W. are co-inventors on a patent application that describes some of the methods reported here.

Conflicts of interest

There are no conflicts to declare.

Acknowledgements

We thank Dr. Ian Swyer, Dr. Michael Dryden, and Alexandros Sklavounos (Univ. Toronto) for fruitful discussions. We thank the Natural Sciences and Engineering Research Council (NSERC) and Abbott Laboratories for funding. J. L. thanks the Canadian Institutes for Health Research (CIHR) for a Vanier Canada Graduate Scholarship. A. R. W. thanks the Canada Research Chair (CRC) program for a CRC.

References

1 C. D. Chin, T. Laksanasopin, Y. K. Cheung, D. Steinmiller, V. Linder, H. Parsa, J. Wang, H. Moore, R. Rouse and G. Umviligihozo, *et al.*, *Nat. Med.*, 2011, **17**(8), 1015–1019.
2 T. Laksanasopin, T. W. Guo, S. Nayak, A. A. Sridhara, S. Xie, O. O. Olowookere, P. Cadinu, F. Meng, N. H. Chee and J. Kim, *et al.*, *Sci. Transl. Med.*, 2015, **7**(273), 273re1.
3 J. Reboud, G. Xu, A. Garrett, M. Adriko, Z. Yang, E. M. Tukahebwa, C. Rowell and J. M. Cooper, *Proc. Natl. Acad. Sci. U. S. A.*, 2019, **116**(11), 4834.
4 S. Sharma, J. Zapatero-Rodríguez, P. Estrela and R. O'Kennedy, *Biosensors*, 2015, **5**(3), 577–601.
5 L. Magro, B. Jacquelin, C. Escadafal, P. Garneret, A. Kwasiborski, J.-C. Manuguerra, F. Monti, A. Sakuntabhai, J. Vanhomwegen and P. Lafaye, *et al.*, *Sci. Rep.*, 2017, **7**(1), 1–9.
6 M. L. Chiu, W. Lawi, S. T. Snyder, P. K. Wong, J. C. Liao and V. Gau, *JALA*, 2010, **15**(3), 233–242.
7 W. Ammerlaan, J.-P. Trezzi, P. Lescuyer, C. Mathay, K. Hiller and F. Betsou, *Biopreserv. Biobanking*, 2014, **12**(4), 269–280.
8 M. S. Bhamla, B. Benson, C. Chai, G. Katsikis, A. Johri and M. Prakash, *Nat. Biomed. Eng.*, 2017, **1**(1), 0009.
9 R. Fan, O. Vermesh, A. Srivastava, B. K. H. Yen, L. Qin, H. Ahmad, G. A. Kwong, C.-C. Liu, J. Gould and L. Hood, *et al.*, *Nat. Biotechnol.*, 2008, **26**(12), 1373–1378.
10 E. Sollier, M. Cubizolles, Y. Fouillet and J.-L. Achard, *Biomed. Microdevices*, 2010, **12**(3), 485–497.
11 L. Qin, O. Vermesh, Q. Shi and J. R. Heath, *Lab Chip*, 2009, **9**(14), 2016–2020.
12 C. Szydzik, K. Khoshmanesh, A. Mitchell and C. Karnutsch, *Biomicrofluidics*, 2015, **9**(6), 064120.
13 C.-C. Chen, P.-H. Lin and C.-K. Chung, *Lab Chip*, 2014, **14**(12), 1996–2001.
14 A. Lenshof, A. Ahmad-Tajudin, K. Järås, A.-M. Swärd-Nilsson, L. Åberg, G. Marko-Varga, J. Malm, H. Lilja and T. Laurell, *Anal. Chem.*, 2009, **81**(15), 6030–6037.
15 B. Seok Lee, J.-N. Lee, J.-M. Park, J.-G. Lee, S. Kim, Y.-K. Cho and C. Ko, *Lab Chip*, 2009, **9**(11), 1548–1555.
16 J. Hauser, G. Lenk, S. Ullah, O. Beck, G. Stemme and N. Roxhed, *Analytical Chemistry*, 2019.
17 S. Wang, D. Sarenac, M. H. Chen, S.-H. Huang, F. F. Giguel, D. R. Kuritzkes and U. Demirci, *Int. J. Nanomed.*, 2012, **7**, 5019–5028.
18 C. Liu, S.-C. Liao, J. Song, M. G. Mauk, X. Li, G. Wu, D. Ge, R. M. Greenberg, S. Yang and H. H. Bau, *Lab Chip*, 2016, **16**(3), 553–560.
19 I. Swyer, S. von der Ecken, B. Wu, A. Jenne, R. Soong, F. Vincent, D. Schmidig, T. Frei, F. Busse and H. J. Stronks, *et al.*, *Lab Chip*, 2019, **19**(4), 641–653.
20 R. P. S. de Campos, D. G. Rackus, R. Shih, C. Zhao, X. Liu and A. R. Wheeler, *Anal. Chem.*, 2019, **91**(3), 2506–2515.
21 Y. Yu, R. P. S. de Campos, S. Hong, D. L. Krastev, S. Sadanand, Y. Leung and A. R. Wheeler, *Microsyst. Nanoeng.*, 2019, **5**(1), 10.
22 J.-L. He, A.-T. Chen, J.-H. Lee and S.-K. Fan, *Int. J. Mol. Sci.*, 2015, **16**(9), 22319–22332.
23 B. F. Bender, A. P. Aijian and R. L. Garrell, *Lab Chip*, 2016, **16**(8), 1505–1513.
24 A. H. C. Ng, M. Lee, K. Choi, A. T. Fischer, J. M. Robinson and A. R. Wheeler, *Clin. Chem.*, 2015, **61**(2), 420–429.
25 C. Dixon, A. H. C. Ng, R. Fobel, M. B. Miltenburg and A. R. Wheeler, *Lab Chip*, 2016, **16**(23), 4560–4568.

26 D. G. Pyne, J. Liu, M. Abdelgawad and Y. Sun, *PLoS One*, 2014, **9**(9), e108128.
27 L. Coudron, M. B. McDonnell, I. Munro, D. K. McCluskey, I. D. Johnston, C. K. L. Tan and M. C. Tracey, *Biosens. Bioelectron.*, 2019, **128**, 52–60.
28 A. H. C. Ng, R. Fobel, C. Fobel, J. Lamanna, D. G. Rackus, A. Summers, C. Dixon, M. D. M. Dryden, C. Lam and M. Ho, *et al.*, *Sci. Transl. Med.*, 2018, **10**(438), eaar6076.
29 R. S. Sista, R. Ng, M. Nuffer, M. Basmajian, J. Coyne, J. Elderbroom, D. Hull, K. Kay, M. Krishnamurthy and C. Roberts, *et al.*, *Diagnostics*, 2020, **10**(1), 21.
30 S. Moon, H. O. Keles, A. Ozcan, A. Khademhosseini, E. Hæggstrom, D. Kuritzkes and U. Demirci, *Biosens. Bioelectron.*, 2009, **24**(11), 3208–3214.
31 S. Wang, X. Zhao, I. Khimji, R. Akbas, W. Qiu, D. Edwards, D. W. Cramer, B. Ye and U. Demirci, *Lab Chip*, 2011, **11**(20), 3411–3418.
32 T. Humphreys, J. Andersson, U. Södervall and T. Melvin, *J. Micromech. Microeng.*, 2009, **19**(10), 105024.
33 J. Liu, C. Hansen and S. R. Quake, *Anal. Chem.*, 2003, **75**(18), 4718–4723.
34 K. W. Oh, C. Park, K. Namkoong, J. Kim, K.-S. Ock, S. Kim, Y.-A. Kim, Y.-K. Cho and C. Ko, *Lab Chip*, 2005, **5**(8), 845–850.
35 R. Fobel, C. Fobel and A. R. Wheeler, *Appl. Phys. Lett.*, 2013, **102**(19), 193513.
36 I. Swyer, R. Fobel and A. R. Wheeler, *Langmuir*, 2019, **35**(15), 5342–5352.
37 M. Kersaudy-Kerhoas and E. Sollier, *Lab Chip*, 2013, **13**(17), 3323–3346.
38 M. J. Schertzer, R. Ben-Mrad and P. E. Sullivan, *J. Microelectromech. Syst.*, 2011, **20**(4), 1010–1015.
39 D. G. Rackus, R. P. S. de Campos, C. Chan, M. M. Karcz, B. Seale, T. Narahari, C. Dixon, M. D. Chamberlain and A. R. Wheeler, *Lab Chip*, 2017, **17**(13), 2272–2280.
40 J. C. Linnes, N. M. Rodriguez, L. Liu and C. M. Klapperich, *Biomed. Microdevices*, 2016, **18**(2), 30.
41 *Polyethersulfone Membrane (Hydrophilic)*, available at https://shop.pall.com/us/en/medical/infusion-therapy/oem-manufacturing/polyethersulfone-membrane-hydrophilic–zidgri78lte, n.d.
42 J. Pavie, A. Rachline, B. Loze, L. Niedbalski, C. Delaugerre, E. Laforgerie, J.-C. Plantier, W. Rozenbaum, S. Chevret and J.-M. Molina, *et al.*, *PLoS One*, 2010, **5**(7), e11581.
43 V. N. Luk, L. K. Fiddes, V. M. Luk, E. Kumacheva and A. R. Wheeler, *Proteomics*, 2012, **12**(9), 1310–1318.
44 L. K. Fiddes, V. N. Luk, S. H. Au, A. H. C. Ng, V. Luk, E. Kumacheva and A. R. Wheeler, *Biomicrofluidics*, 2012, **6**(1), 014112.
45 I. A. Eydelnant, B. B. Li and A. R. Wheeler, *Nat. Commun.*, 2014, **5**(1), 1–9.
46 G. Sathyanarayanan, M. Haapala, I. Kiiski and T. Sikanen, *Anal. Bioanal. Chem.*, 2018, **410**, 6677–6687.
47 H. Yang, J. M. Mudrik, M. J. Jebrail and A. R. Wheeler, *Anal. Chem.*, 2011, **83**(10), 3824–3830.
48 J. M. Mudrik, M. D. M. Dryden, N. M. Lafrenière and A. R. Wheeler, *Can. J. Chem.*, 2014, **92**(3), 179–185.
49 M. J. Jebrail, H. Yang, J. M. Mudrik, N. M. Lafrenière, C. McRoberts, O. Y. Al-Dirbashi, L. Fisher, P. Chakraborty and A. R. Wheeler, *Lab Chip*, 2011, **11**(19), 3218–3224.
50 S. C. C. Shih, H. Yang, M. J. Jebrail, R. Fobel, N. McIntosh, O. Y. Al-Dirbashi, P. Chakraborty and A. R. Wheeler, *Anal. Chem.*, 2012, **84**(8), 3731–3738.
51 S. Mukherjee, T. G. Kang, Y. Chen and S. Kim, *Crit. Rev. Biomed. Eng.*, 2009, **37**(6), 517–529.
52 J. Simoni, G. Simoni, C. D. Lox, S. D. Prien and G. T. Shires, *Anal. Chim. Acta*, 1995, **313**(1), 1–14.
53 S. O. Sowemimo-Coker, *Transfus. Med. Rev.*, 2002, **16**(1), 46–60.
54 O. Fortunato, M. Boeri, C. Verri, D. Conte, M. Mensah, P. Suatoni, U. Pastorino and G. Sozzi, *Molecules*, 2014, **19**(3), 3038–3054.
55 M. B. Kirschner, S. C. Kao, J. J. Edelman, N. J. Armstrong, M. P. Vallely, N. van Zandwijk and G. Reid, *PLoS One*, 2011, **6**(9), e24145.
56 S. Sun, Y. Yue, X. Huang and D. Meng, *J. Membr. Sci.*, 2003, **222**(1), 3–18.
57 E. R. Schwarz, *Curr. Opin. Virol.*, 2017, **27**, 71–77.
58 S. N. Crooke, I. H. Haralambieva, D. E. Grill, I. G. Ovsyannikova, R. B. Kennedy and G. A. Poland, *Vaccine*, 2019, **37**(29), 3876–3882.
59 L. P. Skendzel, *Am. J. Clin. Pathol.*, 1996, **106**(2), 170–174.